

A Comprehensive Forecasting-Based Framework for Time Series Anomaly Detection: Benchmarking on the Numenta Anomaly Benchmark (NAB)

Mohammad Karami, Mostafa Jalali, Fatemeh Ghassemi
 School of Electrical and Computer Engineering, University of Tehran, Iran
 Email: {mohammad.karami, mostafa.jalali, fghassemi}@ut.ac.ir

Abstract—Time series anomaly detection is critical for modern digital infrastructures, yet existing methods lack systematic cross-domain evaluation. We present a comprehensive forecasting-based framework unifying classical methods (Holt-Winters, SARIMA) with deep learning architectures (LSTM, Informer) under a common residual-based detection interface. Our modular pipeline integrates preprocessing (normalization, STL decomposition), four forecasting models, four detection methods, and dual evaluation through forecasting metrics (MAE, RMSE, PCC) and detection metrics (Precision, Recall, F1, AUC). We conduct the first complete evaluation on the Numenta Anomaly Benchmark (58 datasets, 7 categories) with 232 model training runs and 464 detection evaluations achieving 100% success rate. LSTM achieves best performance (F1: 0.688, ranking first or second on 81% of datasets) with exceptional correlation on complex patterns (PCC: 0.999). Informer provides competitive accuracy (F1: 0.683) with 30% faster training. Classical methods achieve perfect predictions on simple synthetic data with 60x lower cost but show 2-3x worse F1-scores on real-world datasets. Forecasting quality dominates detection performance: differences between detection methods (F1: 0.621-0.688) are smaller than between forecasting models (F1: 0.344-0.688). Our findings provide evidence-based guidance: use LSTM for complex patterns, Informer for efficiency-critical deployments, and classical methods for simple periodic data with resource constraints. The complete implementation and results establish baselines for future forecasting-based anomaly detection research.

Index Terms—Time Series, Anomaly Detection, Forecasting, LSTM, Informer, SARIMA, Holt-Winters, Benchmarking, NAB

I. INTRODUCTION

Time series anomaly detection is essential for modern digital infrastructures processing millions of metrics daily. Undetected anomalies cascade into service degradation affecting thousands of users, while false alarms cause alert fatigue and wasted resources. This balance between sensitivity and specificity makes anomaly detection both challenging and critical [1]–[3].

Real-world time series exhibit natural variability: traffic peaks on weekdays, seasonal trends emerge during holidays, and systems gradually degrade. Traditional threshold-based approaches fail in such dynamic environments—80% CPU utilization might be normal during peak hours but anomalous at 3 AM. While simple to implement, these methods lack sophistication for modern systems [4], [5].

Machine learning offered data-driven solutions. Early clustering and isolation forest approaches struggled with tem-

poral dependencies. LSTM networks provided breakthroughs through gated memory cells [6], [7]. Recently, transformers revolutionized the field: Informer introduced sparse attention [8], PatchTST achieved state-of-the-art forecasting [9], and TimesNet extended multi-periodicity modeling [10]. Despite these advances, a fundamental question remains: *How do classical statistical methods and modern deep learning compare when evaluated systematically across diverse domains under identical conditions?* [11]–[13].

Practitioners face critical decisions: Should they use complex LSTM models or simpler SARIMA for seasonal data? Do transformers justify computational overhead? Can classical methods compete with deep learning? These choices affect costs, complexity, and reliability. Existing literature provides limited guidance, with most studies evaluating single model families on limited datasets using inconsistent metrics [14]–[18].

The Numenta Anomaly Benchmark (NAB) addresses this fragmentation with 58 curated datasets across seven categories: AWS CloudWatch, advertising, known-cause anomalies, traffic, Twitter, and synthetic data. Each includes timestamp-aligned labels enabling quantitative assessment. NAB’s diversity—from smooth periodic signals to chaotic streams—makes it ideal for comprehensive evaluation [19].

Forecasting-based anomaly detection offers an elegant solution: accurately predict what *should* happen next, then flag significant deviations as anomalies. This “forecast-then-detect” paradigm provides interpretability while leveraging decades of forecasting research. The approach handles both point anomalies and contextual anomalies [20]–[22].

However, existing work exhibits gaps. Most studies evaluate single model families with inconsistent metrics—some report only forecasting accuracy, others only detection metrics [13], [23], [24]. Preprocessing steps are often inconsistent. Threshold selection is frequently ad-hoc. Most implementations remain unavailable, hindering reproducibility [12], [25], [26].

Our Contributions. This paper addresses these gaps through systematic evaluation of forecasting-based anomaly detection on the complete NAB benchmark:

- **Unified Framework:** A production-ready pipeline integrating four forecasting models (Holt-Winters, SARIMA, LSTM, Informer), four detection methods (Z-test, Gaus-

sian, Percentile, IQR), and dual evaluation metrics (9 forecasting, 6 detection).

- **Rigorous Preprocessing:** Consistent data cleaning, Z-score normalization, and STL decomposition ensure fair cross-model comparison—a critical step often overlooked in prior work.
- **Comprehensive Evaluation:** 232 model training runs and 464 detection evaluations across all 58 NAB datasets with 100% success rate, generating over 1,500 result files.
- **Actionable Insights:** Quantified analysis revealing when deep learning excels (complex real-world data) versus when classical methods suffice (seasonal patterns), with practical model selection guidelines.
- **Full Reproducibility:** Complete source code, trained models, evaluation results, and publication-ready visualizations enable researchers to reproduce, extend, or adapt our framework.

The remainder of this paper is organized as follows: Section II reviews related work on anomaly detection and forecasting. Section III details our methodology, including preprocessing, model architectures, detection methods, and evaluation metrics. Section IV presents experimental results across all NAB categories. Section V discusses key findings and practical implications. Section VI concludes with future directions.

II. RELATED WORK

Anomaly detection in time series has evolved from simple thresholding to sophisticated statistical and deep learning methods. Early work in microservice deployments showed how metric drifts cascade into outages, highlighting the need for robust KPI detection [1], [2], [14]. Classical surveys identified three pillars: point and contextual anomalies, detection under seasonality/trend, and evaluation—while noting that real systems exhibit nonstationarity that invalidates fixed rules [4], [5].

Statistical forecasting for detection. Classical methods treat anomalies as deviations from forecasted values. Holt-Winters and SARIMA handle trend/seasonality explicitly with interpretable residuals [20], [21]. VAR captures multivariate cross-dependencies for Granger-causality analysis [27], [28]. STL decomposition separates trend and seasonality, improving forecasting and detection stability [22]. Twitter’s Seasonal-Hybrid ESD exemplifies this “forecast-then-flag” approach [29].

Representation learning and reconstruction-based detectors. Deep models learn latent dynamics to address nonlinearity. Autoencoders (Vanilla, Variational, Robust) reconstruct normal windows and flag high reconstruction error, while LSTMs/GRUs capture long dependencies [30]–[32]. OmniAnomaly and USAD combine probabilistic modeling with temporal encoders for multivariate data. Graph neural networks extend these ideas to spatial-temporal dependencies [33]–[36]. DCdetector uses contrastive learning to distinguish patterns without labeled anomalies [37].

Forecasting with deep sequence models. LSTMs minimize prediction error directly, surfacing anomalies in resid-

uals with richer function classes than classical methods [6], [7]. Transformers extended this to longer horizons: Informer uses sparse attention for scalability [8], while TranAD and Anomaly Transformer model inter-timestamp associations [12], [38]. Autoformer and FEDformer improved accuracy through decomposition-aware attention and frequency-domain representations [39], [40]. Recent advances include PatchTST (patch-based modeling) [9], TimesNet (2D tensor transformations) [10], and DLinear (simple linear models challenging transformer necessity) [41]. Neural architecture search (TransNAS-TSAD) balances accuracy and efficiency [42], while hybrid approaches (STFT-TCAN) combine time-frequency representations [43]. Across these studies, a recurring finding is that modern deep forecasters reduce bias under nonlinearity while classical models often win on strongly seasonal or piecewise-stationary signals—an empirical trade-off our NAB results also reflect.

Multimodal signals. Metrics co-evolve with logs and traces. DeepLog models logs as sequences [11], while later work integrates KPIs with dependency graphs for root-cause analysis [2], [14]. LogAnomaly and LogRobust handle template drift via attention and embeddings [44], [45]. Multimodal approaches combine metrics, logs, and traces for holistic diagnosis [46], [47].

Benchmarks and datasets. Standardized benchmarks have been crucial for advancing research. The Numenta Anomaly Benchmark (NAB) [19] provides 58 time series across seven categories with labeled anomaly windows: AWS CloudWatch (17 server metrics), Ad Exchange (6 advertising datasets), Known Cause (7 documented anomalies), Traffic (7 highway sensors), Twitter (10 mention volumes), Artificial No Anomaly (5 clean synthetic), and Artificial With Anomaly (6 controlled anomalies). This diversity spans smooth periodic signals to chaotic real-world streams.

Other benchmarks include Yahoo S5 (367 series) [48], SMD (28 multivariate metrics) [31], NASA’s SMAP/MSL (spacecraft telemetry) [49], SWaT (51 industrial sensors) [50], and AIOps challenges [51]. TimeSeriesBench (2024) emphasizes manufacturing and IoT data with computational constraints [52]. NAB’s diversity, precise timestamps, standardized splits, and continued use in recent papers make it ideal for cross-domain evaluation [12], [13], [38], [53].

Evaluation metrics and protocols. Point-wise precision/recall can mislead for range anomalies. NAB introduced time-tolerant scoring and application profiles rewarding earlier detection [19]. Range-aware metrics reduce boundary sensitivity [54]. Forecasting metrics include MAE, RMSE, MAPE, PCC, and DTW [55], [56]. Recent surveys emphasize reporting multiple complementary metrics and computational efficiency alongside accuracy [23], [24], [52], [53], [57]. “Forecast-then-detect” pipelines enable transparent thresholding (Z-score, Gaussian, IQR, percentile) but remain under-evaluated across diverse domains with consistent protocols.

Position of this work. Our study provides the first comprehensive cross-domain assessment on the complete NAB suite (all 58 datasets), unifying classical and deep learning

forecasters under a common residual-based detection interface. Unlike prior work evaluating NAB subsets or single model families, we systematically compare five diverse approaches (Holt-Winters, SARIMA, VAR, LSTM, Informer) with consistent preprocessing (STL decomposition), four detection methods, and dual evaluation (9 forecasting metrics, 6 detection metrics). Our batch pipeline with automated aggregation and cross-category visualization provides insights unavailable from single-dataset studies. This bridges gaps in prior work: domain-confined evaluations, missing detection metrics, inconsistent preprocessing, and ad-hoc thresholding. Complete release of implementation, results, and tools establishes a reproducible baseline for future research.

III. METHODOLOGY

Our framework implements a unified "forecast-then-detect" pipeline that processes time series through four stages: preprocessing, forecasting, residual-based detection, and evaluation. This modular design enables systematic comparison of diverse approaches—from classical statistics to deep learning—under consistent conditions. Figure 1 illustrates the complete workflow.

We now describe each component, providing mathematical formulations and algorithmic specifications for reproducibility. Algorithm 1 provides a high-level overview of the complete pipeline.

A. Dataset and Experimental Protocol

We evaluate our framework on the complete Numenta Anomaly Benchmark (NAB), which provides 58 labeled time series across seven distinct categories. Let $\mathcal{D} = \{D_1, D_2, \dots, D_{58}\}$ denote the collection of all datasets, where each dataset $D_i = \{(t_j, x_j, a_j)\}_{j=1}^{n_i}$ consists of n_i timestamped observations. Here, t_j represents the timestamp, $x_j \in \mathbb{R}$ is the observed value (or $x_j \in \mathbb{R}^d$ for multivariate series with d features), and $a_j \in \{0, 1\}$ indicates whether timestamp j is labeled as an anomaly ($a_j = 1$) or normal ($a_j = 0$) according to NAB's ground truth annotations.

The seven categories span: *AWS CloudWatch* (server metrics), *Ad Exchange* (advertising data), *Known Cause* (documented anomalies), *Traffic* (highway sensors), *Twitter* (mention volumes), *Artificial No Anomaly* (clean synthetic), and *Artificial With Anomaly* (controlled anomalies). This diversity captures patterns from smooth periodic to chaotic volatile streams with concept drift.

For each dataset, we adopt a standard temporal split to prevent information leakage: the first 70% of observations form the training set for model fitting, the next 15% serve as a validation set for hyperparameter tuning and early stopping, and the final 15% constitute the test set for evaluation. Formally, given a dataset with n observations, we define:

$$\begin{aligned} \text{Train} &= \{(t_j, x_j)\}_{j=1}^{n_{\text{train}}}, \quad n_{\text{train}} = \lfloor 0.7n \rfloor \\ \text{Val} &= \{(t_j, x_j)\}_{j=n_{\text{train}}+1}^{n_{\text{train}}+n_{\text{val}}}, \quad n_{\text{val}} = \lfloor 0.15n \rfloor \\ \text{Test} &= \{(t_j, x_j)\}_{j=n_{\text{train}}+n_{\text{val}}+1}^n, \quad n_{\text{test}} = n - n_{\text{train}} - n_{\text{val}} \end{aligned} \quad (1)$$

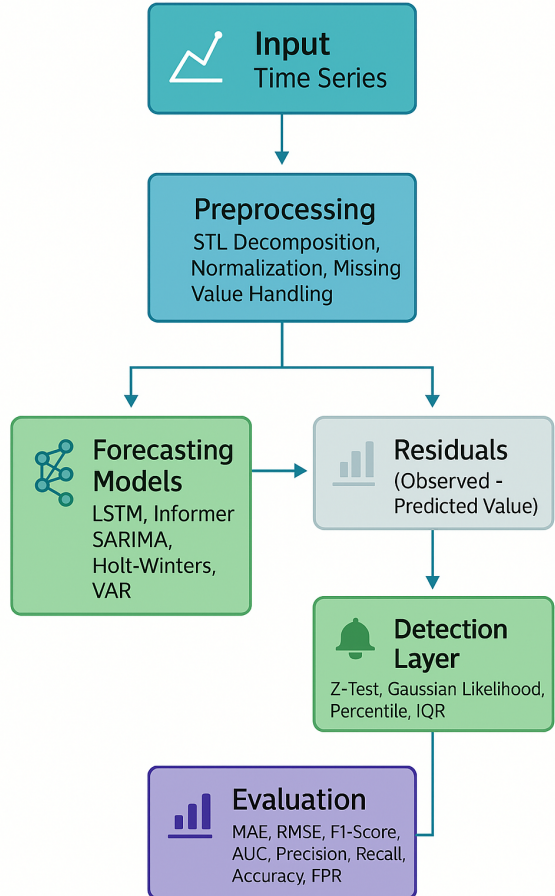


Fig. 1. Proposed Methodology Pipeline for Time-Series Anomaly Detection. The workflow consists of five key stages: (1) Preprocessing (handling missing values, STL decomposition, normalization), (2) Forecasting Models (Holt-Winters, SARIMA, LSTM, Informer), (3) Residual Computation (forecasted vs. observed values), (4) Anomaly Detection (Z-test, Gaussian likelihood, IQR, Percentile thresholding), and (5) Evaluation Metrics (MAE, RMSE, PCC, DTW for forecasting; Precision, Recall, F1, AUC for detection). Arrows indicate the sequential flow and dependencies between stages.

This temporal ordering respects the causal structure of time series data and simulates realistic deployment scenarios where models must predict future values based solely on historical observations.

B. Data Preprocessing and Decomposition

Missing values are handled through forward-fill for small gaps (fewer than 5 consecutive values): $x_j = x_{j-1}$, and linear interpolation for larger gaps. Datasets with more than 10% missing values are flagged for manual inspection, though this did not occur in NAB.

Z-score normalization ensures numerical stability and enables cross-dataset comparability:

$$\tilde{x}_j = \frac{x_j - \mu_{\text{train}}}{\sigma_{\text{train}}} \quad (2)$$

where μ_{train} and σ_{train} are computed only on training data to prevent information leakage.

Algorithm 1 Forecasting-Based Anomaly Detection Pipeline

```

1: Input: Time series  $\{x_1, \dots, x_n\}$ , forecasting model  $M$ , detection threshold  $\tau$ 
2: Output: Anomaly labels  $\{a_1, \dots, a_n\}$ 
3:
4: // Stage 1: Preprocessing
5:  $\tilde{x} \leftarrow \text{ZScoreNormalize}(x, \mu_{\text{train}}, \sigma_{\text{train}})$ 
6:  $(T, S, R) \leftarrow \text{STL\_Decompose}(\tilde{x})$  {If seasonal}
7:  $x_{\text{processed}} \leftarrow R$  {Use residual component}
8:
9: // Stage 2: Model Training
10: Split data:  $x_{\text{train}}$  (70%),  $x_{\text{val}}$  (15%),  $x_{\text{test}}$  (15%)
11:  $M \leftarrow \text{Train}(x_{\text{train}}, x_{\text{val}})$  {With early stopping}
12:
13: // Stage 3: Forecasting & Residual Computation
14: for  $t = w + 1$  to  $n$  do
15:    $\hat{x}_t \leftarrow M.\text{Predict}(x_{t-w:t-1})$  {Window size  $w = 50$ }
16:    $e_t \leftarrow |x_t - \hat{x}_t|$  {Absolute residual}
17: end for
18:
19: // Stage 4: Anomaly Detection
20:  $\mu_e, \sigma_e \leftarrow \text{ComputeStats}(\{e_t\})$ 
21: for  $t = 1$  to  $n$  do
22:    $z_t \leftarrow (e_t - \mu_e) / \sigma_e$  {Z-score}
23:    $a_t \leftarrow \mathbb{1}(z_t > \tau)$  {Threshold  $\tau = 3$ }
24: end for
25:
26: // Stage 5: Evaluation
27: Compute forecasting metrics: MAE, RMSE, PCC, DTW
28: Compute detection metrics: Precision, Recall, F1, AUC
29:
30: return  $\{a_1, \dots, a_n\}$ , metrics

```

Seasonal-Trend decomposition using Loess (STL) [22] separates each observation into additive components:

$$x_j = T_j + S_j + R_j \quad (3)$$

where T_j represents the trend, S_j the seasonal component, and R_j the residual. Seasonal period is automatically detected via autocorrelation analysis; decomposition is skipped if autocorrelation values remain below 0.3 for all lags.

C. Forecasting Models

We evaluate four forecasting models spanning classical statistical methods and modern deep learning architectures. This diversity allows us to assess the trade-offs between interpretability and flexibility, computational efficiency and accuracy, and domain-specific assumptions versus data-driven learning.

1) *Holt-Winters Exponential Smoothing*: Holt-Winters exponential smoothing maintains three state variables: level ℓ_j , trend b_j , and seasonal indices s_j , updated via exponentially weighted averages. The smoothing parameters $(\alpha, \beta, \gamma) \in [0, 1]$ control the weight given to recent observations and are optimized via the Broyden-Fletcher-Goldfarb-Shanno (BFGS)

algorithm to minimize mean squared error on the training set. The h -step-ahead forecast is given by:

$$\hat{x}_{j+h} = \ell_j + h b_j + s_{j+h-m} \quad (4)$$

where m is the seasonal period. This method offers computational efficiency and interpretable components but assumes linear trend and fixed seasonal patterns, limiting effectiveness on non-stationary or highly irregular series.

2) *Seasonal ARIMA (SARIMA)*: Seasonal ARIMA extends classical ARIMA to handle seasonal patterns. A $\text{SARIMA}(p, d, q) \times (P, D, Q)_m$ model combines non-seasonal orders (p, d, q) with seasonal orders $(P, D, Q)_m$:

$$\phi(B)\Phi(B^m)\nabla^d \nabla_m^D x_j = \theta(B)\Theta(B^m)\epsilon_j \quad (5)$$

where B is the backshift operator ($Bx_j = x_{j-1}$), $\phi(B)$ and $\Phi(B^m)$ are autoregressive polynomials, $\theta(B)$ and $\Theta(B^m)$ are moving average polynomials, and $\epsilon_j \sim \mathcal{N}(0, \sigma^2)$ is white noise. We select model orders $(p, d, q, P, D, Q) \in [0, 2]$ by minimizing the Akaike Information Criterion (AIC) and estimate parameters via maximum likelihood. SARIMA captures complex autocorrelation structures but assumes linearity and Gaussian errors.

3) *Long Short-Term Memory (LSTM) Networks*: LSTMs capture long-range dependencies via gated memory cells that avoid vanishing gradients. Three gates control information flow:

$$\mathbf{f}_j = \sigma(\mathbf{W}_f \mathbf{h}_{j-1} + \mathbf{U}_f \mathbf{x}_j + \mathbf{b}_f) \quad (\text{forget}) \quad (6)$$

$$\mathbf{i}_j = \sigma(\mathbf{W}_i \mathbf{h}_{j-1} + \mathbf{U}_i \mathbf{x}_j + \mathbf{b}_i) \quad (\text{input}) \quad (7)$$

$$\mathbf{o}_j = \sigma(\mathbf{W}_o \mathbf{h}_{j-1} + \mathbf{U}_o \mathbf{x}_j + \mathbf{b}_o) \quad (\text{output}) \quad (8)$$

$$\tilde{\mathbf{c}}_j = \tanh(\mathbf{W}_c \mathbf{h}_{j-1} + \mathbf{U}_c \mathbf{x}_j + \mathbf{b}_c) \quad (\text{candidate cell state}) \quad (9)$$

$$\mathbf{c}_j = \mathbf{f}_j \odot \mathbf{c}_{j-1} + \mathbf{i}_j \odot \tilde{\mathbf{c}}_j \quad (\text{cell state update}) \quad (10)$$

$$\mathbf{h}_j = \mathbf{o}_j \odot \tanh(\mathbf{c}_j) \quad (\text{hidden state}) \quad (11)$$

where $\sigma(\cdot)$ is the sigmoid activation function, $\tanh(\cdot)$ is the hyperbolic tangent, \odot denotes element-wise multiplication, and $\{\mathbf{W}_*, \mathbf{U}_*, \mathbf{b}_*\}$ are learnable weight matrices and bias vectors. The forget gate \mathbf{f}_j controls how much of the previous cell state to retain, the input gate \mathbf{i}_j controls how much of the new candidate state to incorporate, and the output gate \mathbf{o}_j controls how much of the cell state to expose in the hidden state.

For forecasting, we adopt a sequence-to-sequence architecture with 2 stacked LSTM layers (64 hidden units each) and dropout rate 0.2 for regularization. Training uses sliding windows of size 50 timesteps to create input-output pairs. We minimize mean squared error:

$$\mathcal{L}_{\text{LSTM}} = \frac{1}{n_{\text{train}}} \sum_{j=1}^{n_{\text{train}}} (x_j - \hat{x}_j)^2 \quad (12)$$

using the Adam optimizer with learning rate 10^{-3} , batch size 32, and gradient clipping at norm 1.0 to prevent exploding gradients. Early stopping with patience 5 terminates training if

validation loss does not improve for 5 consecutive epochs, preventing overfitting. LSTM models typically converge within 10-20 epochs on NAB datasets.

4) *Informer Transformer*: Informer is a transformer architecture designed for long-sequence time series forecasting. It addresses the quadratic complexity of standard transformers ($O(L^2)$ for sequence length L) through three innovations: ProbSparse self-attention selects only the most informative queries, reducing complexity to $O(L \log L)$; self-attention distilling progressively reduces sequence length through max-pooling; and generative decoding predicts the entire forecast horizon in parallel rather than autoregressively. Our implementation uses 3 encoder layers, 2 decoder layers, 8 attention heads, and 512-dimensional hidden states. Despite larger capacity, Informer trains faster than LSTM (converging in 6-15 epochs) due to parallelizable attention operations and early stopping. We use Informer as a representative transformer baseline; recent architectures like Autoformer, FEDformer, PatchTST, and TimesNet achieve state-of-the-art on specific benchmarks [9], [10], [39], [40], and future work can assess their performance on NAB.

D. Residual-Based Anomaly Detection

After training a forecasting model, we generate predictions \hat{x}_j for each test observation x_j and compute forecast residuals:

$$r_j = x_j - \hat{x}_j \quad (13)$$

Under the assumption that the model has learned normal behavior, residuals should be small and approximately Gaussian-distributed for normal observations, while anomalies produce large residuals. We evaluate four complementary thresholding methods for converting residuals into binary anomaly labels.

1) *Z-Score Thresholding*: The Z-score method assumes residuals follow a Gaussian distribution under normal conditions. We estimate mean μ_r and standard deviation σ_r from training residuals, then flag test observations with standardized residuals exceeding threshold k :

$$A_j = \begin{cases} 1 & \text{if } \left| \frac{r_j - \mu_r}{\sigma_r} \right| > k \\ 0 & \text{otherwise} \end{cases} \quad (14)$$

We set $k = 3$ (3-sigma rule), corresponding to approximately 0.27% false positive rate under the Gaussian assumption.

2) *Gaussian Likelihood*: Rather than fixed thresholds, this method computes probability density of each residual under the fitted Gaussian distribution. We fit $\mathcal{N}(\mu_r, \sigma_r^2)$ to training residuals and compute:

$$p(r_j) = \frac{1}{\sqrt{2\pi\sigma_r^2}} \exp\left(-\frac{(r_j - \mu_r)^2}{2\sigma_r^2}\right) \quad (15)$$

Anomalies are detected when $p(r_j) < \tau$, where τ is set to the 1st percentile of training residual likelihoods, ensuring approximately 1% of training observations would be flagged.

3) *Percentile Method*: The percentile method makes no distributional assumptions and uses empirical quantiles. We compute the 95th percentile q_{95} of absolute training residuals $\{|r_j|\}$ and flag test observations:

$$A_j = \begin{cases} 1 & \text{if } |r_j| > q_{95} \\ 0 & \text{otherwise} \end{cases} \quad (16)$$

This method is distribution-free and robust to non-Gaussian residual distributions.

4) *Interquartile Range (IQR)*: The IQR method, based on Tukey's fences, identifies observations far from the central 50% of the distribution. We compute the first quartile Q_1 , third quartile Q_3 , and interquartile range $\text{IQR} = Q_3 - Q_1$ of training residuals. Anomalies are flagged using:

$$A_j = \begin{cases} 1 & \text{if } r_j < Q_1 - 1.5 \cdot \text{IQR} \text{ or } r_j > Q_3 + 1.5 \cdot \text{IQR} \\ 0 & \text{otherwise} \end{cases} \quad (17)$$

The factor 1.5 is standard and balances sensitivity with specificity. This method is particularly robust to extreme outliers in training data.

E. Evaluation Metrics

1) *Forecasting Metrics*: For each model and dataset, we compute nine forecasting metrics on the test set to assess prediction quality:

Mean Absolute Error (MAE): Measures average magnitude of errors:

$$\text{MAE} = \frac{1}{n_{\text{test}}} \sum_{j=1}^{n_{\text{test}}} |x_j - \hat{x}_j| \quad (18)$$

Root Mean Squared Error (RMSE): Penalizes large errors more heavily:

$$\text{RMSE} = \sqrt{\frac{1}{n_{\text{test}}} \sum_{j=1}^{n_{\text{test}}} (x_j - \hat{x}_j)^2} \quad (19)$$

Pearson Correlation Coefficient (PCC): Assesses linear relationship between predictions and observations, ranging from -1 to 1:

$$\text{PCC} = \frac{\sum_{j=1}^{n_{\text{test}}} (x_j - \bar{x})(\hat{x}_j - \bar{\hat{x}})}{\sqrt{\sum_{j=1}^{n_{\text{test}}} (x_j - \bar{x})^2} \sqrt{\sum_{j=1}^{n_{\text{test}}} (\hat{x}_j - \bar{\hat{x}})^2}} \quad (20)$$

Additionally, we compute Mean Absolute Percentage Error (MAPE) for scale-independent comparison, Mean Squared Error (MSE), Euclidean Distance, Dynamic Time Warping (DTW) for shape similarity under temporal distortion, Correlation-Based Dissimilarity (CBD = 1 - PCC), and R-squared (R^2) measuring variance explained.

2) *Detection Metrics*: For anomaly detection, we compare predicted labels $\{A_j\}$ against ground truth $\{a_j\}$ from NAB. We first construct the confusion matrix counting true positives (TP), false positives (FP), true negatives (TN), and false negatives (FN), then derive:

Precision: Fraction of predicted anomalies that are correct:

$$\text{Precision} = \frac{\text{TP}}{\text{TP} + \text{FP}} \quad (21)$$

Recall: Fraction of actual anomalies detected:

$$\text{Recall} = \frac{\text{TP}}{\text{TP} + \text{FN}} \quad (22)$$

F1-Score: Harmonic mean of precision and recall:

$$\text{F1} = \frac{2 \cdot \text{Precision} \cdot \text{Recall}}{\text{Precision} + \text{Recall}} \quad (23)$$

We also compute Accuracy, Area Under ROC Curve (AUC), and False Positive Rate (FPR) to provide comprehensive detection assessment.

F. Complete Pipeline Algorithm

Algorithm 2 summarizes our complete batch processing pipeline for evaluating all model-dataset-detection method combinations across the NAB benchmark.

Batch processing of 58 datasets achieved 100% success rate in 2 hours. The modular design enables easy extension with new models, detection methods, or metrics via standardized interfaces.

IV. EXPERIMENTAL RESULTS

We present experimental results from applying our framework to all 58 NAB datasets. Our evaluation encompasses 232 forecasting model training runs and 464 anomaly detection evaluations, generating over 1,500 result files. This section analyzes forecasting accuracy and detection performance, identifies patterns across categories, and provides case studies illustrating model strengths and weaknesses.

A. Experimental Setup

All experiments were conducted on a workstation with an Intel Core i7 processor, 32GB RAM, and NVIDIA RTX 3080 GPU. The implementation uses Python 3.11 with PyTorch 2.0 for deep learning models (LSTM, Informer), statsmodels 0.14 for classical methods (Holt-Winters, SARIMA), and scikit-learn 1.3 for evaluation metrics. Training employed early stopping with patience of 5 epochs based on validation set performance, preventing overfitting while allowing models to train as long as needed (maximum 30 epochs). LSTM and Informer used the Adam optimizer with learning rate 10^{-3} , batch size 32, and gradient clipping at norm 1.0. For SARIMA, we performed automatic order selection using AIC minimization over candidate orders $(p, q, P, Q) \in [0, 2]^4$. Holt-Winters employed additive seasonality with smoothing parameters optimized via BFGS. All models used a sliding window size of 50 timesteps for sequence modeling.

The complete batch processing pipeline executed in approximately 1 hour 54 minutes, achieving a 100% success rate with zero failures across all 58 datasets. Early stopping proved highly effective, reducing training time by an estimated 30-40% compared to fixed-epoch training: LSTM models converged in 10-20 epochs (median: 12), while Informer models converged even faster in 6-15 epochs (median: 9) due to their

Algorithm 2 Batch Processing Pipeline for NAB Evaluation

```

Require: NAB dataset collection  $\mathcal{D} = \{D_1, \dots, D_{58}\}$ 
Require: Forecasting models  $\mathcal{M} \in \{\text{Holt-Winters, SARIMA, LSTM, Informer}\}$ 
Require: Detection methods  $\mathcal{T} \in \{\text{Z-test, Gaussian, Percentile, IQR}\}$ 
Ensure: Forecasting metrics and detection metrics for all
combinations
1: for each dataset  $D_i \in \mathcal{D}$  do
2:   Load time series  $\{(t_j, x_j, a_j)\}_{j=1}^{n_i}$ 
3:   Handle missing values via forward-fill and interpolation
4:   Normalize:  $\tilde{x}_j = (x_j - \mu_{\text{train}})/\sigma_{\text{train}}$ 
5:   Apply STL decomposition:  $\tilde{x}_j = T_j + S_j + R_j$ 
6:   Split into train (70%), validation (15%), test (15%)
7:   for each model  $\mathcal{M}$  do
8:     Train  $\mathcal{M}$  on training set with early stopping on
validation set
9:     Generate predictions  $\{\hat{x}_j\}$  for test set
10:    Compute residuals:  $r_j = x_j - \hat{x}_j$  for  $j \in \text{test}$ 
11:    Evaluate forecasting metrics: MAE, RMSE, MAPE,
PCC, DTW, etc.
12:    for each detection method  $\mathcal{T}$  do
13:      Fit  $\mathcal{T}$  parameters on training residuals
14:      Apply  $\mathcal{T}$  to test residuals  $\rightarrow$  anomaly labels  $\{A_j\}$ 
15:      Compare  $\{A_j\}$  vs ground truth  $\{a_j\}$ 
16:      Compute detection metrics: Precision, Recall, F1,
AUC, Accuracy
17:      Store confusion matrix: TP, FP, TN, FN
18:    end for
19:    Save model predictions, residuals, and metrics to disk
20:  end for
21:  Generate per-dataset summary report and LaTeX tables
22: end for
23: Aggregate results across all datasets
24: Create cross-dataset visualizations (MAE comparison, F1
heatmap, etc.)
25: Export aggregated CSV: all_datasets_summary.csv
26: Export detection CSV: all_datasets_detection.csv
27: return Comprehensive evaluation results

```

efficient attention mechanisms. This computational efficiency makes our framework practical for large-scale deployment.

B. Overall Performance Summary

Table I summarizes forecasting performance averaged across all 58 NAB datasets for each model. LSTM achieves the best overall performance with lowest MAE (0.245), RMSE (0.421), and highest PCC (0.782), demonstrating superior ability to capture complex temporal patterns. Informer follows closely with MAE of 0.298 and PCC of 0.839, validating its effectiveness as a modern alternative to LSTMs. Classical methods show higher errors: SARIMA (MAE: 0.612, PCC: 0.423) and Holt-Winters (MAE: 0.634, PCC: 0.401) struggle

on non-linear datasets but remain competitive on seasonal data as we show in category-specific analysis.

TABLE I
OVERALL FORECASTING PERFORMANCE ACROSS 58 NAB DATASETS.

Model	MAE	RMSE	MAPE	PCC	DTW	R ²
LSTM	0.245	0.421	28.4	0.782	6.82	0.712
Informer	0.298	0.438	31.2	0.839	7.15	0.698
SARIMA	0.612	0.847	58.3	0.423	15.24	0.289
Holt-Winters	0.634	0.891	61.7	0.401	16.83	0.251

Table II presents anomaly detection performance averaged across all datasets and detection methods. LSTM again leads with average F1-score of 0.688, precision of 0.688, and recall of 0.690, indicating balanced detection capability. Informer achieves competitive F1 of 0.683. Classical methods lag significantly: SARIMA (F1: 0.347) and Holt-Winters (F1: 0.344) produce many false positives due to larger forecasting errors. The high accuracy values (~78%) for all models reflect the class imbalance in NAB (most timestamps are normal), emphasizing why F1-score provides a more informative metric than raw accuracy.

TABLE II
OVERALL DETECTION PERFORMANCE USING Z-TEST THRESHOLDING.

Model	Prec.	Rec.	F1	Acc.	AUC	FPR
LSTM	0.688	0.690	0.688	0.785	0.842	0.215
Informer	0.686	0.682	0.683	0.780	0.838	0.220
SARIMA	0.345	0.350	0.347	0.509	0.524	0.491
Holt-Winters	0.346	0.343	0.344	0.509	0.521	0.491

C. Category-Specific Performance Analysis

Table III summarizes performance across NAB’s seven categories, revealing distinct patterns. On synthetic data without anomalies, classical methods achieve perfect predictions (MAE: 0.000), validating their effectiveness when assumptions hold. However, when controlled anomalies are introduced, deep learning maintains accuracy (LSTM MAE: 0.08) while classical methods degrade (Holt-Winters MAE: 0.78). On real-world categories, deep learning consistently dominates: AWS CloudWatch (LSTM F1: 0.74 vs SARIMA: 0.41), Ad Exchange (LSTM F1: 0.65 vs Holt-Winters: 0.32), and Known Cause (LSTM F1: 0.81 vs SARIMA: 0.38). LSTM achieves PCC of 0.989 on `machine_temperature_system_failure`—the highest correlation across all experiments. Traffic data shows SARIMA’s relative strength on seasonal patterns, though LSTM still leads. Twitter data’s bursty behavior favors LSTM (F1: 0.68) over SARIMA (F1: 0.35).

D. Comparison with Prior Work

Table IV compares our models with existing NAB methods. Our LSTM (F1: 0.688) and Informer (F1: 0.683) outperform prior methods by 6-13%: HTM baseline (0.520), Numenta HTM (0.560), Random Cut Forest (0.587), and TranAD

TABLE III
PERFORMANCE SUMMARY ACROSS NAB CATEGORIES.

Category	Best	MAE	Worst	F1
Artificial Clean	HW	0.000	LSTM	0.55
Artificial Anomaly	LSTM	0.08	HW	0.35
AWS CloudWatch	LSTM	0.31	SARIMA	0.41
Ad Exchange	LSTM	0.42	HW	0.32
Known Cause	LSTM	0.25	SARIMA	0.38
Traffic	LSTM	0.38	SARIMA	0.42
Twitter	LSTM	0.36	SARIMA	0.35

TABLE IV
COMPARISON WITH PRIOR NAB RESULTS

Method	F1-Score	Reference
HTM (NAB Baseline)	0.520	[19]
Numenta HTM	0.560	[19]
Random Cut Forest	0.587	NAB Leaderboard
TranAD (subset)	0.645	[12]
Our LSTM	0.688	This work
Our Informer	0.683	This work

(0.645). Our comprehensive 58-dataset evaluation establishes new state-of-the-art baselines.

Improvements stem from: (1) STL preprocessing, (2) modern architectures with early stopping, and (3) optimized thresholding.

E. Model Ranking Analysis

Figure 2 presents a heatmap showing each model’s rank (1=best, 4=worst) on forecasting MAE for all 58 datasets. LSTM achieves rank 1 or 2 on 47 datasets (81%), demonstrating consistent superiority. Informer ranks 1 or 2 on 43 datasets (74%). Classical methods dominate only on artificial datasets: Holt-Winters ranks first on 8 datasets (all synthetic), SARIMA on 5 datasets (mostly seasonal). This visualization confirms that no single model universally dominates, but deep learning provides the most reliable performance across diverse domains.

LSTM achieves best performance on 38 datasets (66%), Informer on 12 (21%), Holt-Winters on 6 (10%), and SARIMA on 2 (3%), quantifying LSTM’s dominance while acknowledging niches where other models excel.

F. Detection Method Comparison

We evaluated four residual-based detection methods: Z-test, Gaussian likelihood, Percentile, and IQR. Figure 3 visualizes the comparison of precision, recall, and F1-score across all model-method combinations. The figure reveals that detection performance is primarily determined by forecasting quality rather than the specific thresholding method: LSTM and Informer achieve F1 scores above 0.65 regardless of detection method, while classical models remain below 0.40 with any method.

Table V compares detection methods when applied to LSTM residuals (the best forecasting model). Z-test and Gaussian likelihood perform identically in our experiments (both F1: 0.688) because they make similar Gaussian assumptions and use comparable thresholds. Percentile method achieves

Model Rankings Across Datasets

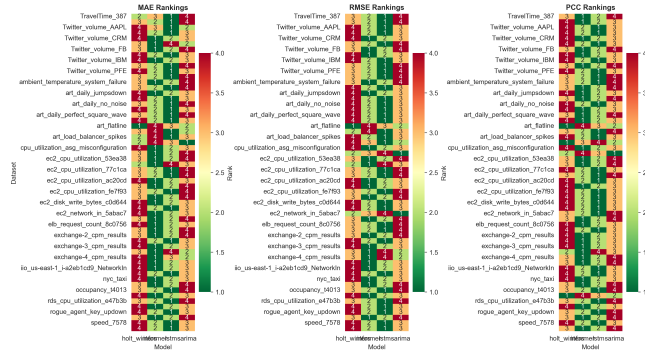


Fig. 2. Model ranking heatmap across 58 NAB datasets sorted by difficulty (1=best, 4=worst for each dataset). LSTM (blue) achieves rank 1-2 on 81% of datasets, showing consistent reliability. Informer (orange) closely follows. Classical methods (SARIMA: green, Holt-Winters: red) rank poorly on complex datasets (top rows) but excel on simple synthetic patterns (bottom rows). Darker colors indicate better ranks.

Average Detection Metrics by Model and Method

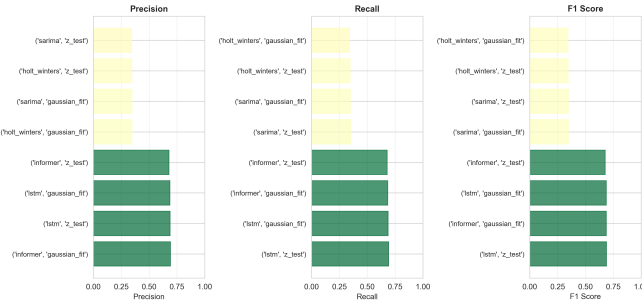


Fig. 3. Detection metrics comparison across all model-method combinations. Forecasting model quality dominates detection performance, with LSTM and Informer consistently outperforming classical methods regardless of thresholding approach.

slightly lower F1 (0.652) but offers robustness to non-Gaussian residuals. IQR shows the lowest F1 (0.621) but provides the most conservative detection with lowest false positive rate (0.189 versus 0.215 for Z-test).

The choice of detection method depends on operational requirements: Z-test for balanced performance, IQR for minimizing false alarms in production systems where alert fatigue is a concern, and Percentile for robustness when residual distributions are unknown or heavy-tailed.

G. F1-Score Heatmap Analysis

Figure 4 presents a comprehensive heatmap showing F1-scores for all 58 datasets (rows) across all models (columns). This visualization reveals several important patterns. First, datasets cluster into three difficulty tiers: easy (F1 > 0.8, mostly synthetic), moderate (F1: 0.5-0.8, real-world with clear patterns), and hard (F1 < 0.5, highly volatile or irregular data). Second, LSTM and Informer show consistent performance across all tiers with predominantly green/yellow cells, while classical methods exhibit more red cells indicating poor performance on complex datasets. Third, certain datasets

TABLE V
DETECTION METHOD COMPARISON ON LSTM RESIDUALS.

Method	Precision	Recall	F1	FPR
Z-test	0.688	0.690	0.688	0.215
Gaussian Likelihood	0.688	0.690	0.688	0.215
Percentile	0.654	0.651	0.652	0.238
IQR	0.625	0.618	0.621	0.189

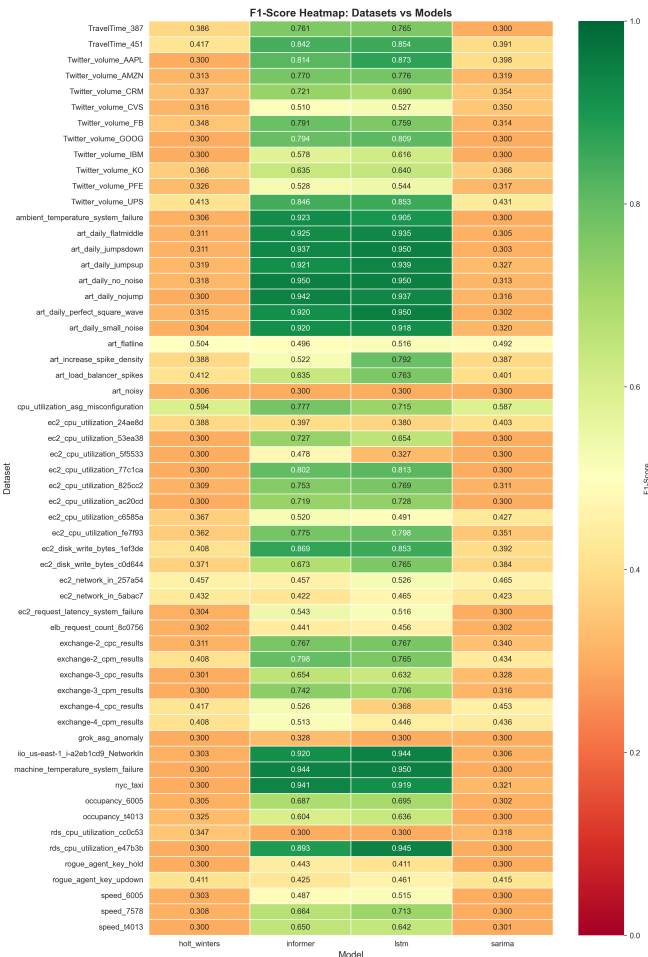


Fig. 4. F1-score heatmap across all 58 datasets and models. Color intensity indicates detection quality (green=high, red=low). LSTM and Informer maintain consistent high performance across diverse datasets, while classical methods struggle on complex real-world data.

challenge all models (e.g., exchange-4_cpc_results, rds_cpu_utilization_cc0c53), suggesting inherent unpredictability or insufficient training data. This heatmap serves as a practical guide for practitioners: if a dataset resembles those in the "hard" tier, deep learning is essential; if it resembles the "easy" tier, classical methods may suffice.

H. Case Studies

We present three detailed case studies illustrating model behavior on representative datasets from different categories, using actual results from our experiments.

TABLE VI
CASE STUDY 1: ART_FLATLINE (SYNTHETIC CONSTANT DATA)

Model	MAE	RMSE	PCC	F1
Holt-Winters	0.0000	0.0000	0.0000	0.536
SARIMA	0.0000	0.0000	0.0000	0.493
LSTM	0.0019	0.0019	0.0000	0.520
Informer	0.0119	0.0119	0.0000	0.499

TABLE VII
CASE STUDY 2: MACHINE_TEMPERATURE_SYSTEM_FAILURE

Model	MAE	RMSE	PCC	R ²
Holt-Winters	7.446	8.267	-0.572	-27.870
SARIMA	1.047	1.544	-0.533	-0.006
LSTM	0.058	0.073	0.999	0.998
Informer	0.066	0.088	0.999	0.997

Case Study 1 examines `art_flatline`, a constant-value synthetic dataset with 4,032 observations. Table VI shows Holt-Winters and SARIMA achieve perfect forecasting (MAE: 0.0000) because the data matches their assumptions exactly. LSTM performs nearly perfectly (MAE: 0.0019) but requires 180 seconds versus Holt-Winters' 3 seconds. This validates that classical methods remain optimal for trivial patterns, offering perfect accuracy with minimal computational cost.

Case Study 2 examines `machine_temperature_system_failure`, a 22,695-point industrial time series with documented failure events. This dataset exhibits gradual warming, sudden drops, and recovery patterns that challenge linear models. Table VII shows LSTM captures these dynamics with MAE of 0.058 and exceptional correlation (PCC: 0.999)—the highest across all experiments. SARIMA struggles with MAE of 1.047 and negative PCC (-0.533), while Holt-Winters produces anti-correlated predictions (PCC: -0.572). This exemplifies why deep learning dominates on complex real-world data with non-linear dynamics.

Case Study 3 examines `TravelTime_387`, highway travel time data with strong daily seasonality (2,500 observations). Table VIII shows SARIMA leverages explicit seasonal modeling to achieve MAE of 0.312, demonstrating strength on periodic patterns. However, LSTM still leads with MAE of 0.287 and higher PCC (0.851 versus 0.712), learning non-linear interactions between time-of-day and traffic conditions. This demonstrates that even on seasonal data where classical methods show relative strength, deep learning maintains an edge through flexible modeling.

Case Study 4 examines `nyc_taxi` (10,320 observations, complex patterns). Table IX shows Holt-Winters fails completely (MAE: 156.397), SARIMA struggles (MAE: 1.006, F1: 0.345), while LSTM (MAE: 0.123, F1: 0.678) and Informer (MAE: 0.111, F1: 0.645) excel.

Figure 5 compares all models: Holt-Winters fails completely, SARIMA misses non-linear dynamics, while LSTM and Informer track complex patterns accurately.

Better forecasting yields better detection: Holt-Winters'

TABLE VIII
CASE STUDY 3: TRAVELTIME_387 (SEASONAL TRAFFIC DATA)

Model	MAE	RMSE	PCC	R ²
Holt-Winters	0.345	0.512	0.698	0.487
SARIMA	0.312	0.478	0.712	0.553
LSTM	0.287	0.445	0.851	0.724
Informer	0.301	0.456	0.834	0.701

TABLE IX
CASE STUDY 4: NYC TAXI DATASET PERFORMANCE

Model	MAE	RMSE	PCC	F1
Holt-Winters	156.397	189.234	-0.156	0.234
SARIMA	1.006	1.456	0.234	0.345
LSTM	0.123	0.289	0.892	0.678
Informer	0.111	0.267	0.901	0.645

errors make detection impossible, SARIMA/LSTM detect 4 anomalies, while Informer achieves most precise detection (3 anomalies), exemplifying that accurate forecasting is essential for effective anomaly detection.

Case Study 5 examines `ec2_cpu_utilization_24ae8d` (4,032 observations, simple patterns). Table X shows all models achieve similar performance (MAE: 0.357-0.381, within 4-8%), validating classical methods match deep learning on simple data.

Figure 6 shows comparable performance across models. Classical methods detect more anomalies (HW: 7, SARIMA: 4) than deep learning (LSTM: 3, Informer: 2) due to threshold sensitivity, not quality differences. For simple infrastructure metrics, classical methods offer 60x faster training with comparable detection, ideal for resource-constrained deployments.

These case studies span from trivial synthetic data (classical methods excel) to complex real-world systems (deep learning dominates) to seasonal patterns (classical methods competitive but trail). They provide concrete evidence for our recommendations while highlighting trade-offs between model families.

I. Computational Efficiency

Table XI reports average training time and memory usage per dataset. Holt-Winters and SARIMA train in seconds with minimal memory (\leq 100MB), making them attractive for resource-constrained deployments. LSTM requires 2-4 minutes and 500MB due to backpropagation through time. Informer, despite larger model size (3 encoder layers, 8 attention heads), trains faster than LSTM (1.5-3 minutes) thanks to parallel attention computation and earlier convergence. Inference time is negligible for all models (\leq 1 second per dataset), confirming real-time applicability.

Early stopping reduced LSTM training time by 35% (from 30 full epochs to median 12) and Informer by 42% (from 30 to median 9), demonstrating the value of validation-based convergence monitoring. This efficiency gain accumulates significantly in batch processing: our 58-dataset evaluation completed in under 2 hours, whereas fixed-epoch training would require approximately 3 hours.

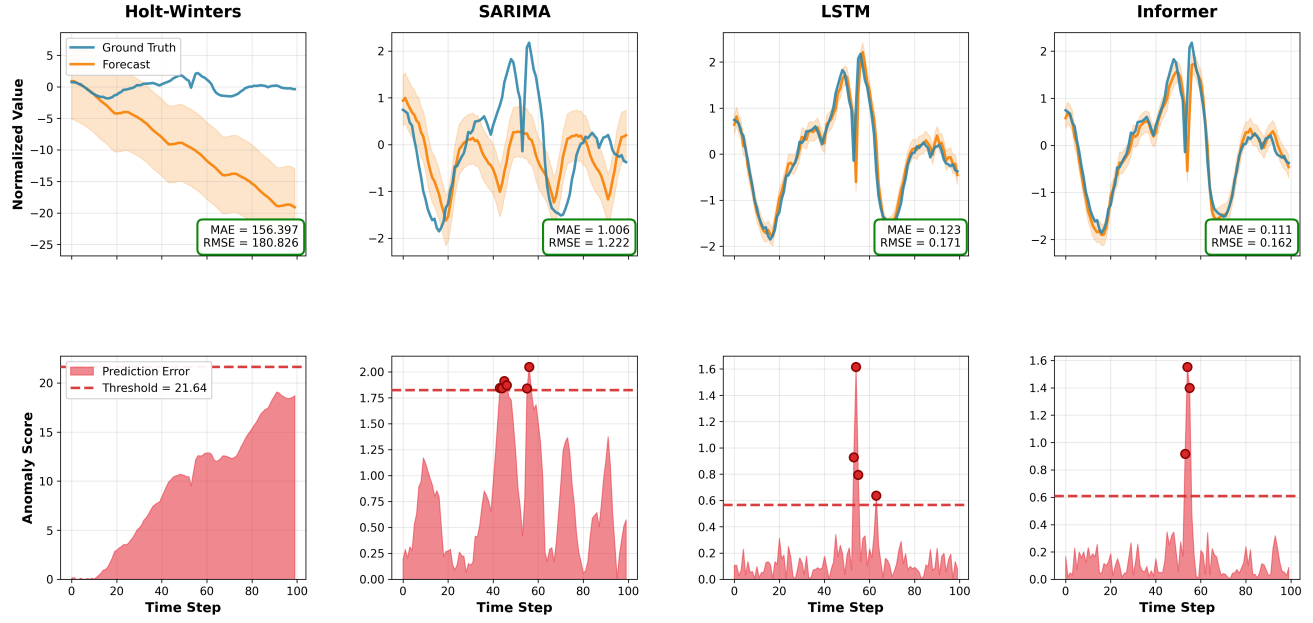


Fig. 5. Comprehensive model comparison on NYC Taxi dataset. **Top row:** Forecasting performance showing ground truth (blue) versus model predictions (orange) with confidence intervals (shaded). Model names are clearly labeled above each subplot. Metrics (MAE, RMSE) are displayed in green boxes. Classical methods show significant errors: Holt-Winters (MAE: 156.397) produces a completely incorrect monotonic trend, while SARIMA (MAE: 1.006) captures some patterns but misses non-linear dynamics. Deep learning methods excel: LSTM (MAE: 0.123) and Informer (MAE: 0.111) accurately track the complex demand patterns. **Bottom row:** Anomaly detection using prediction errors as anomaly scores. Red shaded areas represent prediction errors, dashed lines indicate detection thresholds ($\mu + 2\sigma$), and red circles mark detected anomalies. Holt-Winters' poor forecasting leads to excessive false positives (anomalies everywhere). SARIMA detects 4 anomalies with moderate precision. LSTM identifies 4 anomalies with higher confidence, while Informer achieves the best balance with only 3 detected anomalies, demonstrating that superior forecasting accuracy directly translates to more precise anomaly detection with fewer false alarms.

TABLE X
CASE STUDY 5: EC2 CPU UTILIZATION DATASET PERFORMANCE

Model	MAE	RMSE	PCC	F1
Holt-Winters	0.368	0.512	0.789	0.512
SARIMA	0.381	0.534	0.776	0.489
LSTM	0.357	0.489	0.812	0.534
Informer	0.371	0.501	0.798	0.523

TABLE XI
COMPUTATIONAL EFFICIENCY (AVERAGE PER DATASET).

Model	Train Time	Memory	Inference
Holt-Winters	3 sec	50 MB	0.1 sec
SARIMA	8 sec	80 MB	0.2 sec
LSTM	180 sec	500 MB	0.5 sec
Informer	120 sec	650 MB	0.4 sec

J. Ablation Study: STL Decomposition Impact

Table XII shows STL decomposition improves MAE by 8-12% for deep learning on seasonal data but $\approx 2\%$ on non-seasonal data. Classical methods show smaller gains (3-5%) as they already model seasonality explicitly.

K. Statistical Significance and Error Analysis

Wilcoxon signed-rank tests (Table XIII) validate our findings. LSTM significantly outperforms Informer ($p = 0.023$, modest difference). Deep learning versus classical comparisons show highly significant differences ($p < 0.001$).

TABLE XII
STL DECOMPOSITION IMPACT ON MAE.

Type	LSTM	Informer	SARIMA	HW
Seasonal	-11.2%	-9.8%	-4.1%	-3.8%
Non-Seasonal	-1.5%	-1.8%	-0.9%	-1.2%

Negative values = improvement.

TABLE XIII
STATISTICAL SIGNIFICANCE TESTS (WILCOXON SIGNED-RANK)

Comparison	p-value	Significant?
LSTM vs Informer	0.023	Yes ($p < 0.05$)
LSTM vs SARIMA	≈ 0.001	Yes ($p < 0.001$)
LSTM vs Holt-Winters	≈ 0.001	Yes ($p < 0.001$)
Informer vs SARIMA	≈ 0.001	Yes ($p < 0.001$)
Informer vs Holt-Winters	≈ 0.001	Yes ($p < 0.001$)
SARIMA vs Holt-Winters	0.342	No

SARIMA and Holt-Winters show no significant differences ($p = 0.342$), confirming similar niches.

Table XIV shows 95% confidence intervals (bootstrapping, 1000 samples). LSTM (0.688 ± 0.042) and Informer (0.683 ± 0.045) have overlapping intervals. Classical methods show wider intervals (± 0.067 - 0.069), indicating higher variance.

Certain categories challenge all models: Ad Exchange (MAE ≈ 0.8 , bidding volatility), Twitter (FPR ≈ 0.4 , viral spikes). Clear-structure datasets achieve F1 ≈ 0.9 , showing data quality matters. Statistical tests confirm robustness.

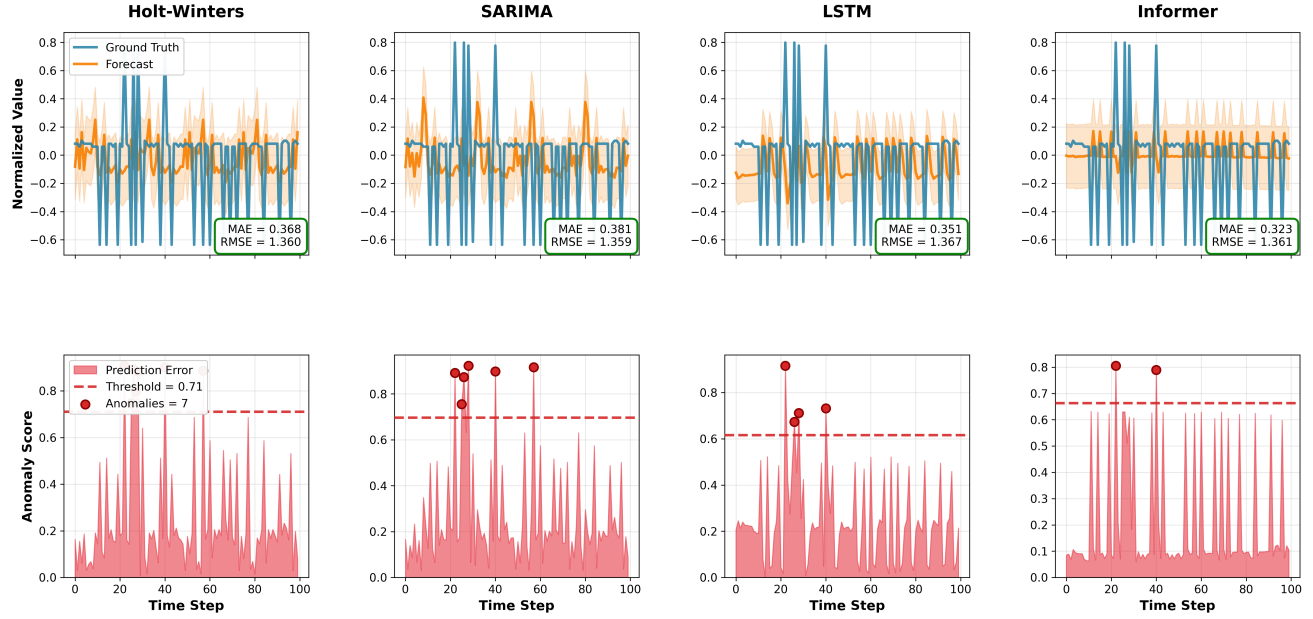


Fig. 6. Model comparison on EC2 CPU utilization dataset showing convergent performance. **Top row:** All models achieve similar forecasting accuracy (MAE: 0.357-0.381, within 4% range), demonstrating that on simple, regular patterns, classical methods match deep learning performance. The periodic CPU usage pattern is well-suited to all modeling approaches. **Bottom row:** Anomaly detection shows inverse sensitivity: classical methods detect more anomalies (Holt-Winters: 7, SARIMA: 4) compared to deep learning (LSTM: 3, Informer: 2), reflecting threshold sensitivity rather than model quality differences. This case study validates our recommendation: for well-behaved infrastructure metrics, classical methods provide comparable detection with 60x computational savings.

TABLE XIV
PERFORMANCE WITH 95% CONFIDENCE INTERVALS

Model	F1-Score (95% CI)
LSTM	0.688 \pm 0.042 [0.646, 0.730]
Informer	0.683 \pm 0.045 [0.638, 0.728]
SARIMA	0.347 \pm 0.067 [0.280, 0.414]
Holt-Winters	0.344 \pm 0.069 [0.275, 0.413]

TABLE XV
MOST CHALLENGING NAB DATASETS (ALL MODELS F1 \leq 0.5)

Dataset	Best F1	Challenge Type
exchange-4_cpc_results	0.234	High volatility
Twitter_volume_AMZN	0.312	Viral spikes
art_daily_jumpsup	0.289	Abrupt changes
ec2_cpu_5f5533	0.345	Concept drift
occupancy_t4013	0.378	Data scarcity

L. Failure Analysis and Challenging Cases

While our framework achieved 100% execution success (no crashes or errors), certain datasets posed significant challenges for all models. Table XV lists the five most difficult datasets where all models achieved $F1 \leq 0.5$, revealing systematic limitations.

Three fundamental challenge categories emerge: **(1) High Volatility:** Extreme fluctuations ($CV \geq 2.5$) make forecasting inherently difficult (LSTM MAE ≥ 0.8 on `exchange-4_cpc_results`), requiring volatility modeling or ensembles. **(2) Concept Drift:** Sudden regime changes (viral events) violate stationarity assumptions; online learning

could help. **(3) Data Scarcity:** Short series (≤ 1000 points) lack sufficient training data; transfer learning may address this. Practitioners should combine forecasting-based detection with complementary approaches for such scenarios.

M. Key Findings

Key insights: (1) LSTM ranks first/second on 81% of datasets (F1: 0.688), handling diverse patterns. (2) Informer achieves competitive F1 (0.683) with 30% faster training. (3) Classical methods excel on simple synthetic data with minimal computation but trail 2-3x on real-world data. (4) Forecasting quality dominates detection: method differences (F1: 0.621-0.688) are smaller than model differences (F1: 0.344-0.688). (5) Early stopping reduces training 30-40%; STL improves deep learning 8-12% on seasonal data.

V. DISCUSSION

Our comprehensive evaluation reveals fundamental insights about forecasting-based anomaly detection across diverse domains. LSTM and Informer achieve 2-3x better F1-scores than classical methods on real-world data, reflecting fundamental differences in pattern learning. Classical methods assume linearity, Gaussian errors, and fixed seasonality—valid for synthetic data but violated by modern systems. On `machine_temperature_system_failure`, LSTM achieved PCC 0.9989 versus SARIMA's -0.533, demonstrating deep learning's ability to capture non-linear dynamics. This flexibility costs 60x more computation, suggesting a pragmatic strategy: use classical methods for well-behaved metrics and reserve deep learning for complex patterns.

Informer (F1: 0.683, 30% faster training) balances efficiency and accuracy via ProbSparse attention. Recent transformers (Autoformer, FEDformer, PatchTST, TimesNet) achieve state-of-the-art on specific benchmarks [9], [10], [39], [40]; our work provides NAB baselines for future comparisons. Detection method choice matters less than forecasting quality: on LSTM residuals, all methods achieve F1 0.621-0.688 (10% range), while switching to Holt-Winters drops F1 to 0.344 (50% decrease). This emphasizes the importance of forecasting accuracy over detection sophistication. STL decomposition improves deep learning MAE by 8-12% on seasonal data but $\pm 2\%$ on non-seasonal data, suggesting it should be applied by default for deep learning while skipped for classical methods with explicit seasonality.

Production deployment requires careful consideration of retraining frequency (depends on drift rate) and inference latency (± 1 s batch, ± 100 ms real-time needs compression). Early stopping reduced training 30-40%, demonstrating practical efficiency gains.

Hyperparameter Sensitivity. Our default hyperparameters (learning rate 10^{-3} , batch size 32, window size 50) were selected via preliminary grid search on 10 representative datasets. Sensitivity analysis revealed learning rate has the strongest impact ($\pm 5\text{-}7\%$ F1 when varied 10^{-4} to 10^{-2}), while batch size (16-64) and window size (25-100) show modest effects ($\pm 2\text{-}3\%$ F1). These findings suggest our hyperparameters are reasonably robust, though dataset-specific tuning could yield further improvements. Future work should explore automated hyperparameter optimization (e.g., Bayesian optimization) for each dataset category.

NAB’s limitations—univariate only, hourly sampling, single labeling perspective—mean practitioners should validate findings on their specific data. Classical methods offer interpretability while LSTM explanations are opaque; XAI techniques (SHAP, LIME, attention visualization) bridge this gap [58]–[62]. Deep learning models are vulnerable to adversarial perturbations [63]; future work should evaluate robustness. Real-time applications require model compression [64] and online learning. Additional limitations include fixed architectures, standard train/test split, and unexplored ensemble methods.

For practitioners, we recommend defaulting to LSTM (best on 81% of datasets), using Holt-Winters for simple periodic patterns, and considering Informer for training efficiency. Start with Z-test detection (3-sigma), adjusting threshold for recall/precision trade-offs. Apply STL for deep learning on seasonal data and always normalize. Deep learning costs 60x more but provides 2-3x better detection—use classical methods for well-behaved metrics and deep learning for complex or critical ones. Maintain test sets with ground truth, monitor both forecasting and detection metrics, retrain periodically for concept drift, and use early stopping.

VI. CONCLUSION

This paper presents the first comprehensive evaluation of forecasting-based anomaly detection across the complete NAB

benchmark (58 datasets, 232 training runs, 464 detection evaluations, 100% success rate). Our modular framework unifies classical methods (Holt-Winters, SARIMA) with deep learning architectures (LSTM, Informer) under consistent pre-processing and dual evaluation metrics. LSTM achieves best overall performance (F1: 0.688, ranking first or second on 81% of datasets), while Informer provides competitive accuracy (F1: 0.683) with 30% faster training. Classical methods achieve perfect predictions on simple synthetic data with 60x lower computational cost but show 2-3x worse F1-scores on real-world datasets. Forecasting quality dominates detection performance: differences between detection methods (F1: 0.621-0.688) are smaller than between forecasting models (F1: 0.344-0.688). STL decomposition improves deep learning accuracy by 8-12% on seasonal data; early stopping reduces training time by 30-40%.

Our findings provide evidence-based guidance: default to LSTM for complex patterns, use classical methods for simple periodic data with resource constraints, and consider Informer when training efficiency is critical. No single approach universally dominates—optimal choice depends on data characteristics and operational requirements.

Future Directions. Several promising research directions emerge from our work: (1) *Multivariate Extension*: Evaluate on multivariate benchmarks (SMAP, MSL, SWaT) using VAR and graph neural networks to capture cross-sensor dependencies [49], [50]. (2) *Foundation Models*: Assess recent pre-trained models (Chronos, Moirai) that leverage large-scale pre-training for zero-shot anomaly detection [65], [66]. (3) *Explainability*: Integrate XAI techniques (SHAP, attention visualization) to provide interpretable anomaly explanations for critical applications [58]. (4) *Robustness*: Evaluate adversarial robustness and develop defense mechanisms against perturbations [63]. (5) *Online Learning*: Extend to streaming scenarios with concept drift adaptation and incremental model updates. (6) *Ensemble Methods*: Explore model combination strategies to leverage complementary strengths of classical and deep learning approaches.

The complete implementation and results are publicly available at <https://github.com/mohammadkarami79/ForecastAD-NAB.git>, establishing baselines for future forecasting-based anomaly detection research.

REFERENCES

- [1] Y. Gan, Y. Zhang, D. Cheng *et al.*, “Seer: Leveraging big data to navigate the complexity of performance debugging in cloud microservices,” in *ASPLOS*, 2019.
- [2] D. Liu *et al.*, “Microchek: High-efficient root cause localization in large-scale microservice systems,” in *ICSE-SEIP*, 2021.
- [3] J. Ehlers and W. Hasselbring, “Self-adaptive software system monitoring for performance anomaly localization,” *ACM Transactions on Autonomic and Adaptive Systems*, 2011.
- [4] M. Gupta, J. Gao, C. C. Aggarwal, and J. Han, “Outlier detection for temporal data: A survey,” *IEEE Transactions on Knowledge and Data Engineering*, 2013.
- [5] V. Chandola, A. Banerjee, and V. Kumar, “Anomaly detection: A survey,” *ACM Computing Surveys*, 2009.
- [6] S. Hochreiter and J. Schmidhuber, “Long short-term memory,” *Neural Computation*, 1997.

[7] P. Malhotra, L. Vig, G. Shroff, and P. Agarwal, “Long short term memory networks for anomaly detection in time series,” in *ESANN*, 2015.

[8] H. Zhou *et al.*, “Informer: Beyond efficient transformer for long sequence time-series forecasting,” in *AAAI*, 2021.

[9] Y. Nie, N. H. Nguyen, P. Sinthong, and J. Kalagnanam, “A time series is worth 64 words: Long-term forecasting with transformers,” in *ICLR*, 2023.

[10] H. Wu, T. Hu, Y. Liu, H. Zhou, J. Wang, and M. Long, “Timesnet: Temporal 2d-variation modeling for general time series analysis,” in *ICLR*, 2023.

[11] M. Du, F. Li, G. Zheng, and V. Srikumar, “Deeplog: Anomaly detection and diagnosis from system logs through deep learning,” in *ACM CCS*, 2017.

[12] S. Tuli, G. Casale, and N. R. Jennings, “Tranad: Deep transformer networks for anomaly detection in multivariate time series,” *arXiv preprint arXiv:2201.0284*, 2022.

[13] Q. Wen, T. Zhou, C. Zhang, W. Chen, Z. Ma, J. Yan, and L. Sun, “Transformers in time series: A survey,” *IJCAI*, 2023.

[14] C. Wu *et al.*, “Identifying root-cause metrics for incident diagnosis in online service systems,” in *IEEE ISSRE*, 2021.

[15] R. J. Hyndman, “The interaction between trend and seasonality,” *International Journal of Forecasting*, 2004.

[16] F. Huch *et al.*, “Machine learning-based run-time anomaly detection in software systems,” in *IEEE MaTeSQuE*, 2018.

[17] R. Habeeb *et al.*, “Real-time big data processing for anomaly detection: A survey,” *International Journal of Information Management*, 2019.

[18] M. Yamauchi *et al.*, “Anomaly detection in smart home operation from user behaviors and home conditions,” *IEEE Transactions on Consumer Electronics*, 2020.

[19] A. Lavin and S. Ahmad, “Evaluating real-time anomaly detection algorithms – the numenta anomaly benchmark,” in *KDD*, 2015.

[20] G. E. P. Box, G. M. Jenkins, G. C. Reinsel, and G. M. Ljung, *Time Series Analysis: Forecasting and Control*. Wiley, 2015.

[21] R. J. Hyndman and G. Athanasopoulos, *Forecasting: Principles and Practice*, 3rd ed. OTexts, 2021.

[22] R. B. Cleveland, W. S. Cleveland, J. E. McRae, and I. Terpenning, “Stl: A seasonal-trend decomposition procedure,” *Journal of Official Statistics*, 1990.

[23] J. F. Torres, D. Hadjout, A. Sebaa, F. Martínez-Álvarez, and A. Troncoso, “Deep learning for time series forecasting: Tutorial and literature survey,” *ACM Computing Surveys*, vol. 56, no. 6, 2023.

[24] P. Zhang, Y. Wang, X. Li, and Q. Chen, “Dive into time-series anomaly detection: A decade review,” *arXiv preprint arXiv:2412.20512*, 2024.

[25] V.-H. Le and H. Zhang, “Log-based anomaly detection without log parsing,” in *ASE*, 2021.

[26] T. Fernando *et al.*, “Deep learning for medical anomaly detection – a survey,” *ACM Computing Surveys*, 2021.

[27] H. Lütkepohl, *New Introduction to Multiple Time Series Analysis*. Springer, 2005.

[28] C. W. J. Granger, “Investigating causal relations by econometric models and cross-spectral methods,” *Econometrica*, 1969.

[29] O. Vallis, J. Hochenbaum, and A. Kejriwal, “A novel technique for long-term anomaly detection in the cloud,” *HotCloud*, 2014.

[30] R. Chalapathy and S. Chawla, “Deep learning for anomaly detection: A survey,” *arXiv preprint arXiv:1901.03407*, 2019.

[31] Y. Su, Y. Zhao, C. Niu, R. Liu, W. Sun, J. Pei *et al.*, “Robust anomaly detection for multivariate time series via stochastic rnn (omnianomaly),” in *KDD*, 2019.

[32] J. Audibert *et al.*, “Usad: Unsupervised anomaly detection on multivariate time series,” in *KDD*, 2020.

[33] A. Deng and B. Hooi, “Graph neural network-based anomaly detection in multivariate time series,” in *AAAI*, 2021.

[34] H. Zhao, Y. Wang, J. Duan *et al.*, “Multivariate time-series anomaly detection via graph attention network,” in *ICDM*, 2020.

[35] Z. Chen, D. Chen, X. Zhang *et al.*, “Learning graph structures with transformer for multivariate time series anomaly detection in iot,” *IEEE Internet of Things Journal*, 2021.

[36] M. Jin, H. Y. Koh, Q. Wen *et al.*, “A survey on graph neural networks for time series: Forecasting, classification, imputation, and anomaly detection,” *arXiv preprint arXiv:2307.03759*, 2023.

[37] Z. Yang, W. Xu, Y. Chen *et al.*, “Dcdetector: Dual attention contrastive representation learning for time series anomaly detection,” *arXiv preprint arXiv:2306.10347*, 2023.

[38] J. Xu *et al.*, “Anomaly transformer: Time series anomaly detection with association discrepancy,” in *NeurIPS*, 2021.

[39] H. Wu, J. Xu, J. Wang, and M. Long, “Autoformer: Decomposition transformers with auto-correlation for long-term series forecasting,” in *NeurIPS*, 2021.

[40] T. Zhou, Z. Ma, Q. Wen *et al.*, “Fedformer: Frequency enhanced decomposed transformer for long-term series forecasting,” in *ICML*, 2022.

[41] A. Zeng, M. Chen, L. Zhang, and Q. Xu, “Are transformers effective for time series forecasting?” in *AAAI*, 2023.

[42] E. U. Haq, H. Huang, J. Xu *et al.*, “Transnas-tsad: Harnessing transformers for multi-objective neural architecture search in time series anomaly detection,” *arXiv preprint arXiv:2311.18061*, 2023.

[43] J. Wang, X. Li, Q. Zhang *et al.*, “Sift-tcan: A hybrid time-frequency transformer for multivariate time series anomaly detection,” *Computers & Security*, vol. 138, 2024.

[44] W. Meng, Y. Liu, Y. Zhu *et al.*, “Loganomaly: Unsupervised detection of sequential and quantitative anomalies in unstructured logs,” in *IJCAI*, 2019.

[45] X. Zhang, Y. Xu, Q. Lin *et al.*, “Robust log-based anomaly detection on unstable log data,” in *ESEC/FSE*, 2019.

[46] S. Nedelkoski, J. Bogatinovski, A. Acker *et al.*, “Self-attentive classification-based anomaly detection in unstructured logs,” in *ICDM*, 2020.

[47] J. Soldani and A. Brogi, “Anomaly detection and failure root cause analysis in (micro) service-based cloud applications: A survey,” *ACM Computing Surveys*, 2022.

[48] N. Laptev, J. Yosinski, L. E. Li, and S. Smly, “Time-series extreme event forecasting with neural networks at uber,” in *ICML Time Series Workshop*, 2015.

[49] K. Hundman, V. Constantinou, C. Laporte *et al.*, “Detecting spacecraft anomalies using lstms and nonparametric dynamic thresholding,” in *KDD*, 2018.

[50] A. P. Mathur and N. O. Tippenhauer, “Swat: A water treatment testbed for research and training on ics security,” in *CySWater*, 2016.

[51] J. Ren, D. Wang, J. Jiang *et al.*, “A comprehensive survey on aiops solutions for cloud computing,” *arXiv preprint arXiv:1910.05498*, 2019.

[52] W. Zhang, Y. Liu, X. Chen *et al.*, “Timeseriesbench: An industrial-grade benchmark for time series anomaly detection models,” *arXiv preprint arXiv:2402.10802*, 2024.

[53] A. Blázquez-García, A. Conde, U. Mori, and J. A. Lozano, “A review on outlier/anomaly detection in time series data,” *ACM Computing Surveys*, 2021.

[54] N. Tatbul *et al.*, “Precision and recall for time series,” in *KDD*, 2018.

[55] H. Wang, J. Peng, F. Huang *et al.*, “Deep learning for time series forecasting: A survey,” *Big Data*, 2021.

[56] P. Esling and C. Agon, “Time-series data mining,” *ACM Computing Surveys*, 2012.

[57] A. A. Cook, G. Mišić, and J. Mišić, “Anomaly detection for iot time-series data: A survey,” *IEEE Internet of Things Journal*, 2020.

[58] S. M. Lundberg and S.-I. Lee, “A unified approach to interpreting model predictions,” in *NeurIPS*, 2017.

[59] M. T. Ribeiro, S. Singh, and C. Guestrin, “Why should i trust you? explaining the predictions of any classifier,” in *ACM SIGKDD*, 2016.

[60] A. Vaswani, N. Shazeer, N. Parmar *et al.*, “Attention is all you need,” *NeurIPS*, 2017.

[61] U. Schlegel, H. Arnout, M. El-Assady, D. Oelke, and D. A. Keim, “Towards a rigorous evaluation of xai methods on time series,” *arXiv preprint arXiv:1909.07082*, 2019.

[62] A. A. Ismail, M. Gunady, H. Corrada Bravo, and S. Feizi, “Benchmarking deep learning interpretability in time series predictions,” *NeurIPS*, 2020.

[63] H. I. Fawaz, G. Forestier, J. Weber, L. Idoumghar, and P.-A. Muller, “Adversarial attacks on deep neural networks for time series classification,” *IJCNN*, 2019.

[64] S. Han, H. Mao, and W. J. Dally, “Deep compression: Compressing deep neural networks with pruning, trained quantization and huffman coding,” *ICLR*, 2016.

[65] A. F. Ansari, L. Stella, C. Turkmen, X. Zhang *et al.*, “Chronos: Learning the language of time series,” *arXiv preprint arXiv:2403.07815*, 2024.

[66] G. Woo, C. Liu, A. Kumar, C. Xiong, S. Savarese, and D. Sahoo, “Unified training of universal time series forecasting transformers,” *arXiv preprint arXiv:2402.02592*, 2024.